Experiments in Fluids 32 (2002) 683–688 © Springer-Verlag 2002
DOI 10.1007/s00348-002-0419-6

# Measuring concentrations with laser-induced thermalization and electrostriction gratings

**S. Schlamp, T.H. Sobota**



**Abstract** Laser-induced thermal acoustics is used to measure non-intrusively the concentration of a resonantly excited seed species diluted within a non-resonantly excited species by comparing the contributions from thermalization and electrostriction in the combined signal. The speed of sound is measured simultaneously. It is shown theoretically and experimentally (for iodine vapor in nitrogen) that the ratio of the grating magnitudes of the thermal and of electrostrictive gratings is proportional to the concentration of the resonantly excited species. The proportionality constant only depends on the two species. The uncertainty is 5% when thermal and electrostrictive contributions are comparable in magnitude. The speed of sound is measured simultaneously with an uncertainty of 0.35%.

## Introduction

Flow luminosity, harsh environments, and short test times limit the number of options for flow diagnostic techniques in combustion processes and hypersonic applications. Because of usage of incoherent light emission or scattering effects, linear laser diagnostic techniques are sensitive to flow luminosity, such as emitted in combustion processes. Laser-induced fluorescence (LIF) and Raman scattering, for example, which are commonly used for concentration measurements (McDonell and Samuelsen 2000), belong to the group of linear techniques. Signal levels in conventional Raman scattering are very low so that this technique is most sensitive to flow luminosity. LIF has been demonstrated in shock tube experiments but failed for high flow enthalpies where flow luminosity becomes important (Palma et al. 1998).

*Received: 21 September 2000 / Accepted: 21 December 2001*
*Published online: 17 April 2002*

S. Schlamp (✉)
Graduate Aeronautical Laboratories
California Institute of Technology
Pasadena, CA 91125, USA
E-mail: schlamp@ifd.mavt.ethz.ch
Tel.: +41-1-6325124
Fax: +41-1-6321147

T.H. Sobota
Advanced Projects Research, Inc., 1925 McKinley Ave.
La Verne, CA 91750, USA

*Present address*: S. Schlamp
ETH Zürich, Institute of Fluid Dynamics
Sonneggstrasse 3, 8092 Zürich, Switzerland

Nonlinear laser diagnostic techniques rely on coherently emitted or scattered light, resulting in a coherent signal beam. In addition to filtering by wavelength, the signal beam can be filtered spatially, reducing noise from flow luminosity. Coherent anti-Stokes Raman scattering (CARS), a nonlinear derivative of Raman scattering, does not provide single-shot data, as some applications require. Dual-line CARS does not have this limitation (Paleat and Lefevre 1991). CARS has been demonstrated in super-, hypersonic, and chemically reacting flows (Anderson and Eckbreth 1992).

Laser-induced thermal acoustics (LITA) is a nonlinear laser diagnostic technique that has been developed by Cummings (Cummings 1995) for use in the T5 hypervelocity shock tube (Hornung 1992) at the California Institute of Technology. It is capable of measuring the speed of sound (Butenhoff 1995) and the thermal diffusivity (e.g., Schlamp et al. 2000c) of a gas. If the speed of sound–temperature dependence is known, such as for a perfect gas, LITA can perform thermometry (e.g., Brown and Roberts 1999). Velocimetry using LITA in subsonic (e.g., Hemmerling et al. 1999) and supersonic (Schlamp 2000) flows has also been demonstrated using heterodyne and homodyne detection, respectively. The test gas can be excited resonantly (e.g., Walker et al. 1998) or non-resonantly (e.g., Stampanoni-Panariello et al. 1998). In this paper the application of LITA for the measurement of concentrations is demonstrated. The speed of sound is measured simultaneously. If used with a LITA velocimetry setup, the flow velocity, speed of sound, and a species concentration can be measured simultaneously, instantaneously, non-intrusively, and remotely at a single point in the flow.

Two coherent pulsed laser beams (excitation beams) intersect at their foci inside the sample volume where an interference grating is created. If the test gas absorbs energy at the excitation wavelength (by a mechanism called thermalization) the electric field grating results in a stationary thermal grating and two initially identical acoustic waves, which offset the thermal grating initially. Subsequently, the acoustic waves travel in opposite directions (Cummings et al. 1995). Electrostriction is a mechanism by which molecules are accelerated along electric field gradients by an induced dipole moment. In this case, two acoustic waves of opposite sign, which travel in opposite directions, are created. Density changes also change the index of refraction. Therefore, the evolution and interactions of the waves can be observed by a continuous laser beam (interrogation beam) directed at the Bragg angle at the sample volume. Depending on the instanta-

neous modulation depth of the refractive index grating, part of the interrogation beam is scattered into a coherent signal beam. If the grating is convected with the flow, then the signal beam is Doppler-shifted relative to the interrogation beam. Heterodyne detection of the signal and a reference beam allows LITA velocimetry. The time history of the signal beam is recorded and represents a LITA signal.

Figure 1 shows examples of LITA signals. Figure 1a is a LITA signal that is observed when the test gas is excited resonantly (thermalization signal). Figure 1f gives the signal, at otherwise identical conditions, if excitation occurs non-resonantly (electrostriction signal). The speed of sound is encoded in the oscillation (ringing) frequency in the early parts of the signal. The two different mechanisms result in different ringing frequencies. The ringing frequency for the signal in Fig. 1f is twice that of the signal in Fig. 1a. The signal tail in Fig. 1a is due to the stationary thermal density grating and its decay is governed by thermal diffusion. The decay time constant is inversely proportional to the thermal diffusivity. The tail will extend over longer times in high-pressure gases where the thermal diffusivity is small. This tail is not present in purely electrostrictive signals. The decay behavior for electrostrictive signals such as in Fig. 1f is governed by the finite-size beam geometry.

If the excitation occurs by both molecular mechanisms simultaneously, then different contributions to the signal can be distinguished (Fig. 1b–e). If the wavelength of the excitation laser is such that only one species in a mixture of gases is excited resonantly, then the strength of the resonant contribution to the total signal can be related to the concentration of the resonant species. This is demonstrated with the binary mixture of iodine vapor diluted in nitrogen.



## Theory

The LITA signal amplitude from test gases where thermalization is negligible (Fig. 1f) is proportional to the square of the number density of the non-resonant species molecules (Cummings 1995)

$$L_e \propto \rho_{nr}^2 \tag{1}$$

Similarly, if thermalization is much stronger than electrostriction (Fig. 1a), then the signal amplitude grows with the square of the number density of the resonant species(Cummings 1995)

$$L_\theta \propto \rho_r^2 \tag{2}$$

If electrostrictive and thermal density gratings are comparable in strength (Fig. 1c–e) then

$$L_{\theta+e} \neq L_\theta + L_e \tag{3}$$

i.e., the resulting LITA signal is not the linear superposition of the thermalization and the electrostriction signals. This is due to nonlinear interaction between the electrostrictive and the thermal density gratings.

The first, third, etc., peaks in Fig. 1c–e stem only from electrostriction. The second, fourth, etc., peaks are superpositions of electrostrictive and thermalization peaks. The ratio of the peak heights is not a simple function of the concentration (Fig. 2). Furthermore, finite-rate thermalization (the thermalization rate is a function of the density and becomes very large for high densities) and thermal diffusion (the thermal diffusivity decreases with increasing density) also influence the peak heights. This makes the simple comparison of peak heights unsuitable for concentration measurements. The nonlinear interactions between thermal and electrostrictive gratings are also visible from the temporal shift of the peaks as a function of varying importance of thermalization as compared to electrostriction (Fig. 3).

For a more general analysis consider a binary mixture of perfect gases. The gas susceptibility of the mixture, $\chi_m$, at frequency $\omega$ is then

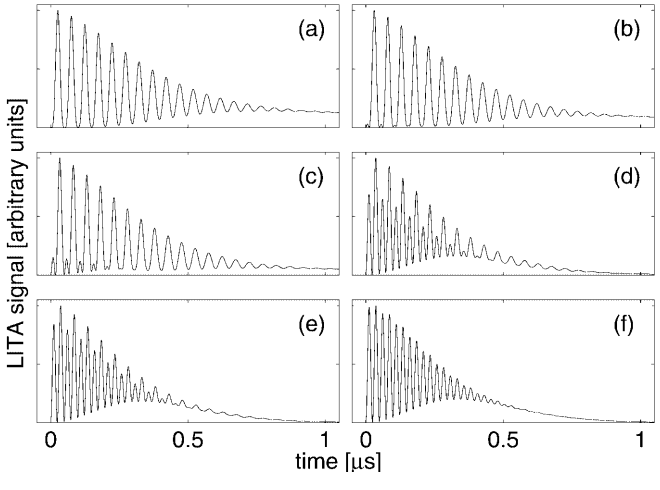


**Fig. 1a–f.** Normalized LITA signals for different values of $U_\theta/U_e$; **a** $R$=5.0, **b** 1.0, **c** 0.5, **d** 0.1, **e** 0.05, **f** 0.01

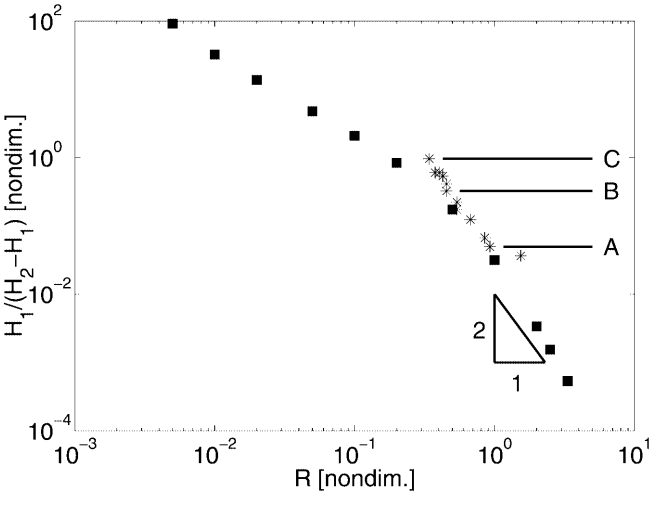


**Fig. 2.** Ratio of peak heights vs $R$ (*solid square* represents values calculated from theory in Cummings et al. 1995) for zero thermal diffusion and infinite thermalization rate, *asterisk* denotes experimental data). $H_1$ denotes the amplitude of the first purely electrostrictive peak if present (e.g., first peak in Fig. 1c). $H_2$ is the amplitude of the first mixed peak (e.g., first peak in Fig. 1a or the second peak in Fig. 1c). The symbols labeled A–C correspond to the raw data plotted in Fig. 4a–c

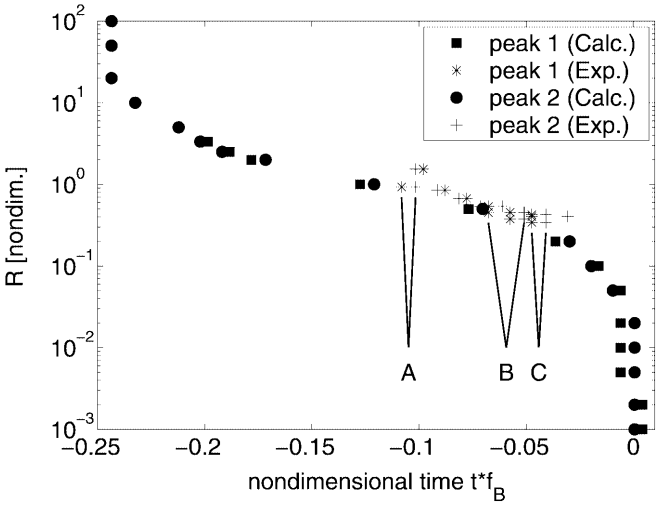


**Fig. 3a–c.** Location of first pure electrostrictive peak and first mixed peak as function of $R$ (*solid square* and *solid circle* are values calculated from theory in Cummings et al. (1995) for zero thermal diffusion and infinite thermalization rate, *asterisk* and *plus* represent experimental data). Above $R \approx 4$, the signal does not contain purely electrostrictive peaks. The time is nondimensionalized with $f_B$, the grating's Brillouin frequency, for generality (here: $f_B$=20.3 MHz). The maximum peak shift in the experimental data is ≈10 ns. The symbols labeled A–C correspond to the raw data plotted in Fig. 4a–c

$$\chi_m(\omega) = \frac{\rho_1}{\rho_1+\rho_2}\chi_1(\omega) + \frac{\rho_2}{\rho_1+\rho_2}\chi_2(\omega) \tag{4}$$

where $\rho_i$ denotes the molecule number density of gas $i$. The approximate modulation depth of the electrostrictive gratings, $U_e$, is proportional to the real part of the gas susceptibility of the test gas at the excitation laser frequency, $\omega_d$, i.e.,

$$U_e \propto \Re\{\chi_m(\omega_d)\} \tag{5}$$

The modulation depth of the thermal gratings, $U_\theta$, is proportional to the imaginary part of the gas susceptibility,

$$U_\theta \propto \Im\{\chi_m(\omega_d)\} \tag{6}$$

Substituting Eq. (2) into Eqs. (5) and (6) yields

$$U_e \propto \frac{\rho_1}{\rho_1+\rho_2}\Re\{\chi_1(\omega_d)\} + \frac{\rho_2}{\rho_1+\rho_2}\Re\{\chi_2(\omega_d)\} \tag{7}$$

$$U_\theta \propto \frac{\rho_1}{\rho_1+\rho_2}\Im\{\chi_1(\omega_d)\} + \frac{\rho_2}{\rho_1+\rho_2}\Im\{\chi_2(\omega_d)\} \tag{8}$$

Define the ratio $R$ as

$$R \equiv \frac{U_\theta}{U_e} = \frac{\rho_1\Im\{\chi_1(\omega_d)\} + \rho_2\Im\{\chi_2(\omega_d)\}}{\rho_1\Re\{\chi_1(\omega_d)\} + \rho_2\Re\{\chi_2(\omega_d)\}} \tag{9}$$

Consider now the case where gas 1 is a seed species, such that

$$\rho_1 \ll \rho_2 \tag{10}$$

Assume furthermore that only gas 1 is excited resonantly. Gas 2 is excited non-resonantly only,

$$\rho_1\Im\{\chi_1(\omega_d)\} \gg \rho_2\Im\{\chi_2(\omega_d)\} \tag{11}$$

i.e., the energy absorption of species 2 is negligible compared to the energy absorption of species 1. Equation (9) then simplifies to

$$R \approx \frac{\rho_1\Im\{\chi_1(\omega_d)\}}{\rho_2\Re\{\chi_2(\omega_d)\}} \approx \frac{\rho_1}{\rho_1+\rho_2}\frac{\Im\{\chi_1(\omega_d)\}}{\Re\{\chi_2(\omega_d)\}} \propto c \tag{12}$$

where $c$ is the concentration of the resonant seed species in the mixture. Hence, under the condition formulated in Eq. (11), $U_\theta/U_e$ is proportional to the concentration of the resonant seed species. The proportionality constant only depends on the two gases and the excitation frequency, but (owing to line broadening at high temperatures and pressures) only weakly on the thermodynamic state of the gas mixture. Binary mixtures satisfying Eqs. (10) and (11) for visible wavelengths are for example $NO_2$/air and $I_2$/air. The analysis also holds if the non-resonant species is itself a mixture of different gases, none of which absorbs energy at the excitation laser frequency. If the condition in Eq. (10) does not hold, then Eq. (12) has to be modified. For concentration measurements to be possible, it is only necessary that the complex gas susceptibilities are linearly independent.

Cummings et al. (1995) introduce $U_\theta$ and $U_e$, which can be seen as dimensionless density grating magnitudes caused by thermalization and electrostriction respectively, as parameters in their theoretical treatment for LITA. Given the theoretical model as given in Cummings et al. (1995) or Schlamp et al. (2000b) and experimental data, $U_\theta$ and $U_e$ can be found by a nonlinear fit of the model to the data with $U_\theta$ and $U_e$ as free parameters. With those and the proportionality constant, the concentration can be found. This constant is a function of $\chi_1(\omega_d)$ and $\chi_2(\omega_d)$ so that it will be different for each combination of gases. However, a calibration measurement at a single known concentration, which yields the constant, is sufficient to establish the relationship between the concentration and $R$. If the assumptions used in the derivation for Eq. (12) do not hold, then a calibration curve has to be determined by measurements over the entire range of concentrations of interest.

## Experiments

A frequency-doubled, Q-switched Nd:YAG laser (Continuum Surelite I10, maximum of 250 mJ at 532 nm, 9 ns pulse duration, 10 Hz repetition rate) was used as the excitation laser. The Q-switch delay was set to adjust the pulse energy to approximately 20 mJ per pulse. A 50/50 beam splitter split the beam in halves, which were focused path-length matched onto a point in the center of the test section where they intersected at an angle of 1.74°. The fringe spacing of the interference grating is hence 18 μm. The Gaussian beam half-width at the beam waist is 400 μm.

The test section is 200 mm long and 50 mm in inside diameter. It is equipped with a K-type thermocouple near the center, an electronic pressure sensor (Omega Engineering PX302–300AV, 0–20 bar), and a mixing fan. The thermocouple provides the input for a temperature controller (Cole Palmer, Temperature Controller R/S), which regulates the power supplied to two resistance

heating blankets (60 W each) on the outside of the test section. Windows provide optical access on both ends of the test section.

A cw $Ar^+$-laser (Spectra-Physics Stabilite 2017, maximum of 1.3 W at 488 nm, operated at 0.2 W in power-controlled mode) provides the interrogation beam. The scattered signal beam passes through an interference filter and a spatial filter to eliminate contributions from ambient light, incoherently scattered light, and from the excitation laser pulse. A photomultiplier tube (Hamamatsu H5783–03, 0.65 ns response time) detects the filtered signal beam. The signal is recorded at 2,048 time-discretized points with 12-bit resolution on a digital storage oscilloscope (Hewlett-Packard Infinium, 500 MHz sampling rate) and subsequently transferred to a personal computer for storage and data analysis.



Iodine vapor is used as resonant species. It has a peak in its spectrum at 532.107 nm (Simmons and Hougen 1977) compared with the wavelength of the Nd:YAG laser of 532.08 nm with a line width of 1 $cm^{-1}$. Hence, only a small (but sufficient) fraction of the energy falls on the absorption line. At room temperature, iodine is solid and sublimates to create a low vapor pressure. The vapor pressure is a function of temperature only. It provides a convenient way to add low concentrations of gaseous iodine quantitatively. The vapor pressure changes by three orders of magnitude between 273 and 373 K, so that the desired partial pressure of iodine can be regulated over a wide range by adjusting the temperature. The vapor pressure of iodine at a temperature of 303 K is 60 Pa (West and Astle 1982). Nitrogen was used as a non-resonant species to dilute the iodine vapor.

A few solid crystals (in the order of 100 mg) of iodine are placed inside the test section. The ambient air is then washed out of the test section by repeatedly pressurizing the test section with nitrogen and draining back to ambient pressure. The solid iodine is given 60 min to sublimate until the equilibrium is reached. Thirty-two shot-averaged LITA signals are then recorded at increasing total pressures (approximately every 0.3 bar). A wait time of 1 min after every addition of nitrogen ensures the proper mixture of the iodine and the nitrogen, and that the temperature is constant for all measurements. The maximum pressure is 15.7 bar. All experiments are conducted at a temperature of 303 K. The mixer inside the test section operates continuously.

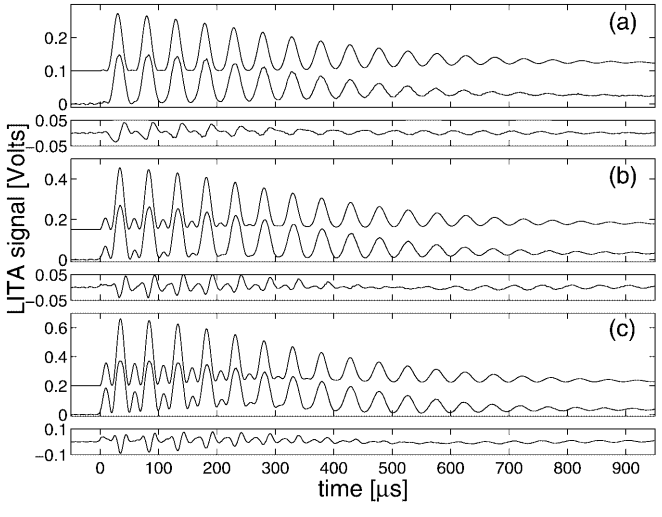


**Fig. 4a–c.** Measured and fitted theoretical (shifted for clarity) signals for different iodine vapor concentrations; **a** 115.5 ppm, **b** 60 ppm, **c** 40.5 ppm. The residual between the fitted signal and the data is plotted below each pair of traces

The Levenberg–Marquardt scheme (Press 1988) is used for a least-squares fit of the theoretical model as given in Cummings et al. (1995) to the data (Fig. 4). A calibration measurement, which yields the beam-crossing angle and the Gaussian beam half-widths, is performed in the test section filled with nitrogen at atmospheric pressure and 303 K. The speed of sound and the thermal diffusivity are here known and held fixed in the fitting procedure. In later measurements, the beam-crossing angle and the beam sizes were held constant and the speed of sound, the thermal diffusivity, $U_e$, and $U_\theta$ were the floating fitting parameters. At atmospheric conditions, the thermalization rate for nitrogen is approximately 39 MHz. The rate increases rapidly for higher pressures. To limit the dimensionality of the parameter space in the fitting, infinitely fast thermalization is assumed.

## Results

Figure 2 demonstrates that the superposition of electrostrictive and thermalization signal contributions is not linear. For signals with both types of peaks, Fig. 2 plots the ratio of the first peak's amplitude, $H_1$, to the difference in amplitude between the first two peaks, $H_2$–$H_1$. If the superposition were linear then by subtracting the electrostrictive peak height from the mixed second peak should result in the amplitude that a pure thermalization signal would have (neglecting thermal diffusion and finite beam-size effects, which should be negligible in the time scales in which the first two peaks are observed, as well as finite-rate thermalization). The symbols in Fig. 2 should then fall on a line with a slope of –2 (in a log–log plot). This behavior is observed only for negligible electrostriction. The reason is nonlinear interactions, mathematically represented by cross terms $U_\theta U_e$ in addition to the terms that scale with $U_\theta^2$ and $U_e^2$ (Cummings et al. 1995). Experimental results match the theoretical predictions well. For $R$>1, the electrostrictive contributions are very weak, which increases the uncertainty of $R$ (see also Fig. 5). Noise becomes comparable to the height $H_1$ of the first peak. These two effects can explain the outlier at $R\approx1.5$. The points around point C ($R\approx0.3$) lie consistently above the theoretical curve. Finite-rate thermalization reduces the height of the second peak compared with its height if the thermalization was instantaneous. The assumption of instantaneous thermalization should improve for smaller values of $R$ (high pressures). Instead, a deviation is seen in this range, but not for larger $R$ (lower pressures). This is because for larger $R$, $H_1$ increases, and the difference $H_2$–$H_1$ thus becomes smaller so that underestimating $H_2$ results in higher errors than it does for larger values of $R$ where $H_1$ is very small.

The nonlinearity is also evident from Fig. 3, which shows a temporal shift for the first two peaks of a mixed LITA signal. The location of the peaks for pure electro-

striction signals is used as a reference. The shift is such that peaks occur at earlier times with increasing importance of thermalization (increasing $R$). The extrema of zero and $-0.25f_B$ are reached asymptotically for $R\rightarrow 8$ and $R\rightarrow 0$, respectively. Subsequent peaks undergo an identical shift but only the first two peaks are plotted. The location of the peaks is nondimensionalized by the Brillouin frequency, $f_B$, of the grating. The shift of $0.25f_B$ occurs between $R$=0.1 and $R$=1.0. For $R$>4, no electrostrictive peak can be detected. All peaks in a given signal should be shifted by the same amount. Slight differences between the two calculated curves are due to the temporal resolution of the calculation (0.5 ns). Signal noise causes additional discrepancies between the peak shifts in the experimental data. The theoretical curves (solid symbols) in Figs. 2 and 3 neglect thermal diffusion and assume infinitely fast thermalization in the calculations. The predicted shift also was observed in the experimental data. In fact, the peak shifting aids in the data analysis in that the error of the least-squares fit is very sensitive towards horizontal offsets of theoretical model and data. In particular for signals with very little electrostriction (Fig. 4a), where the electrostrictive peaks are very weak, the peak shift is the primary measure for $R$.

Three examples for recorded LITA signals at different iodine vapor concentrations are depicted in Fig. 4. Also plotted (shifted for clarity) are the results from the nonlinear fit. The qualitative agreement to the theoretical predictions (Fig. 1) is good. The fitted curves match the measured traces very well, as shown by the residuals that are plotted below each pair of traces.

Figure 5 shows the measured $R$ vs the iodine vapor concentration. As postulated in Eq. (12), the measured $R$ is proportional to the iodine concentration. This relationship seems to break down for concentrations of more than 130 ppm. The higher scatter for higher concentrations is due to the difficulty of accurately capturing weak electrostrictive contributions (e.g., Figs. 1b and 4a). $U_e$ and $U_\theta$ are measured separately. If either of the two becomes very small compared to the other or if the noise level becomes comparable to either then the uncertainty increases dramatically. The deviation of the data in Fig. 5 from the linear relationship is hence not due to the fact that the validity of Eq. (12) breaks down, which should not be the case for concentrations of 130 ppm, but represents a large measurement uncertainty. The inverse of the slope of the solid line is the missing proportionality constant for Eq. (12). The linear regression for this range has an $R^2$ of 0.95 and a standard error of 5%. Part of the scatter is due to fluctuating iodine vapor pressures (scatter in temperature, see also Fig. 6) in the test cell so that the uncertainty of the measurement technique is probably less than 5%. The labels A–C indicate that the point corresponds to the raw data from Fig. 4a–c.



Further reduction of the iodine concentration was not possible because of the pressure rating of the test section and the lack of cooling possibilities of the test section (to avoid condensation on the windows). The temperatures, which were determined from the LITA traces (c.f., Figure 6), had an uncertainty of 0.7% (2 K), which was more than the temperature fluctuations as indicated by the thermocouple (0.16%). The uncertainty level of the LITA measurements is also higher than could be expected at a constant temperature with averaging over 32 signals (Schlamp et al. 2000c). This could be the result of adding one degree of freedom to the fitting procedure. Previous experiments used either thermalization or electrostriction, but not both simultaneously. The vapor pressure grows exponentially with temperature so that part of the scatter of the data around the line in Fig. 5 can be attributed to uncertainties in the true iodine concentration owing to small temperature fluctuations.

The measured sound speeds throughout the experiment are plotted in Fig. 6. The standard deviation of the speed of sound is 0.34%. The speed of sound increases steadily

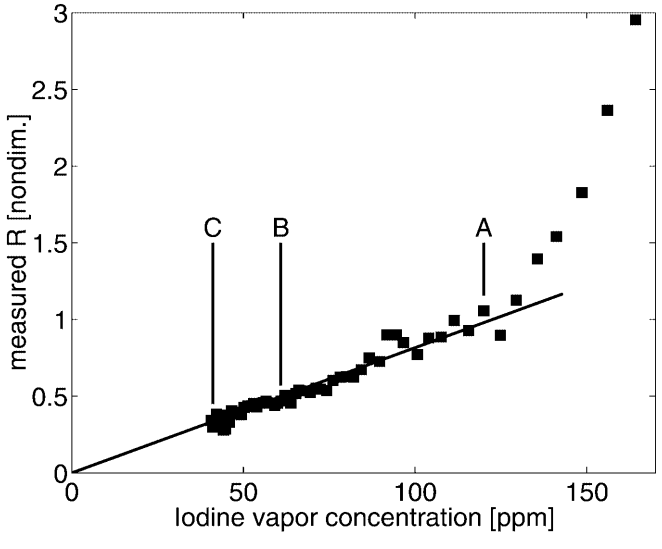


**Fig. 5.** Measured ratio $U_\theta/U_e$ vs iodine vapor concentration. The solid line is a linear regression to the data passing through the origin. The symbols labeled A–C correspond to the raw data plotted in Fig. 4a–c

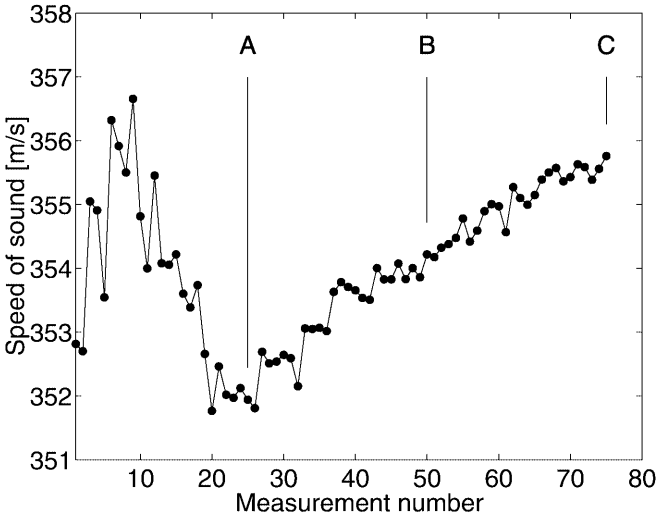


**Fig. 6.** Measured speed of sound throughout experiment from 32 shot-averaged LITA signal. The pressure is increased in steps of ≈0.3 bar between data points. Measurements are taken in time steps of 60 s

during the last two thirds of the test series. This indicates that, despite the constant reading of the thermocouple, the temperature was rising during this phase of the experiment and that the speed of sound measurements is less uncertain than indicated above.

## Conclusions

LITA can be used for concentration measurements in gases by resonantly exciting the trace species of interest and by simultaneous non-resonant excitation of all other species. The electrostrictive contributions of the trace species can be neglected. A proportionality constant has to be determined in a calibration measurement for each combination of trace and dilution species. If the laser cannot be tuned to an absorption band of the species of interest, if other species in the mixture share absorption bands at all achievable wavelengths, or if the species of interest is a majority species, then a tracer can be added. Since the concentration of the tracer within the species of interest is known, the concentration of the species of interest can be determined from the measured concentration of the tracer within the entire gas mixture.

Iodine, for example, is soluble in most fuels and can be used as an additive to study fuel mixing in combustors. The iodine molecule possesses many resonance frequencies in the visible range (Simmons and Hougen 1977). Atmospheric gases as well as common combustion hydrocarbons are transparent at these wavelengths.

To improve accuracy, the grating magnitudes of the thermal and electrostrictive gratings should be comparable. This condition determines the range of applicability for this technique, i.e., the lower and upper bounds for the concentration. The range depends on the species as well as the wavelength of the excitation laser. With the current setup, the concentration of iodine vapor in nitrogen or air can be measured between 10 and 130 ppm, where the lower limit is an estimate. The range can be expanded by increasing the signal-to-noise ratio. If a tracer is used, this is achieved by adjusting the tracer concentration within the species of interest. If the resonant species concentration is fixed, the amount of thermalization can be regulated by tuning the excitation laser only partially onto absorption bands.

While not used here, a combination with heterodyne detection (Schlamp et al. 2000a) allows for simultaneous measurements of speed of sound, concentration, and flow velocity.



## References


Anderson TJ, Eckbreth AC (1992) Simultaneous coherent anti-Stokes–Raman spectroscopy measurements in hydrogen-fueled supersonic combustions. J Propul Pwr 8:7–15

Brown MS, Roberts WL (1999) Single-point thermometry in high-pressure, sooting, premixed combustion environments. J Propul Pwr 15:119–127

Butenhoff TJ (1995) Measurement of the thermal diffusivity and speed of sound of hydrothermal solutions via the laser-induced grating technique. Int J Thermophys 16:1–9

Cummings EB (1995) Laser-induced thermal acoustics. PhD thesis, California Institute of Technology

Cummings EB, Leyva IA, Hornung HG (1995) Laser-induced thermal acoustics (LITA) signals from finite beams. Appl Opt 34:3290–3302

Hemmerling B, Kozlov DN, Stampanoni-Panariello A (1999) Measurement of gas flow velocities by electrostrictive laser-induced gratings. In: Book of abstracts, XVIII European CARS Workshop: CARS and related gas-phase diagnostics, C.R. ENEA, Frascati, Italy, 21–23 March

Hornung HG (1992) Performance data of the new free-piston shock tunnel at GALCIT. AIAA Paper 92–3943

McDonell VG, Samuelsen GS (2000) Measurement of fuel mixing and transport processes in gas turbine combustion. Meas Sci Technol 11:870:886

Palma PC, McIntyre TJ, Houwing AFP (1998) PLIF thermometry in shock tunnel flows using a Raman-shifted tunable excimer laser. Shock Waves 8:275–284

Paleat M, Lefevre M (1991) Temperature measurements by dual-line CARS in low-pressure flows. Appl Phys Lasers Opt 53B:23–29

Press WH (1988) Numerical recipes in C: the art of scientific computing. Cambridge University Press, Cambridge, Mass.

Schlamp S (2000) Laser-induced thermal acoustic velocimetry. PhD thesis, California Institute of Technology

Schlamp S, Cummings EB, Sobota TH (2000a) LITA velocimetry using heterodyne detection. Opt Lett 25:224–226

Schlamp S, Hornung HG, Cummings EB (2000b) Neural network data analysis for laser-induced thermal acoustics. Meas Sci Technol 11:784–794

Schlamp S, Hornung HG, Sobota TH, Cummings EB (2000c) Accuracy and uncertainty of single-shot, nonresonant laser-induced thermal acoustics. Appl Opt 39:5477–5481

Simmons JD, Hougen JT (1977) Atlas of the $I_2$ spectrum from 19,000 to 18,000 $cm^{-1}$. J Res Nat Bur Stand Phys Chem 81A:25

Stampanoni-Panariello A, Hemmerling B, Hubschmid W (1998) Temperature measurements in gases using laser-induced electrostrictive gratings. Appl Phys Lasers Opt 67B:125–130

Walker DJW, Williams RB, Ewert P (1998) Thermal grating velocimetry. Opt Lett 23:1316–1318

West RC, Astle MJ (eds) (1982) Handbook of chemistry and physics, 63rd edn. CRC Press, Boca Raton, Fl